ACS OMEGA

http://pubs.acs.org/journal/acsodf

Article

Modified Titanium Dioxide as a Potential Visible-Light-Activated Photosensitizer for Bladder Cancer Treatment

Thaiane Robeldo,* Lucas S. Ribeiro, Lida Manrique, Andressa Mayumi Kubo, Elson Longo, Emerson Rodrigues Camargo, and Ricardo Carneiro Borra

Cite This: *ACS Omega* 2022, 7, 17563−17574

Read Online

ACCESS | Metrics & More | Article Recommendations

ABSTRACT: Low oxygen concentration inside the tumor microenvironment represents a major barrier for photodynamic therapy of many malignant tumors, especially urothelial bladder cancer. In this context, titanium dioxide, which has a low cost and can generate high ROS levels regardless of local O_2 concentrations, could be a potential type of photosensitizer for treating this type of cancer. However, the use of UV can be a major disadvantage, since it promotes breakage of the chemical bonds of the DNA molecule on normal tissues. In the present study, we focused on the cytotoxic activities of a new material ($Ti(OH)_4$) capable of absorbing visible light and producing high amounts of ROS. We used the malignant bladder cell line MB49 to evaluate the effects of multiple concentrations of $Ti(OH)_4$ on the cytotoxicity, proliferation, migration, and production of ROS. In addition, the mechanisms of cell death were investigated using FACS, accumulation of lysosomal acid vacuoles, caspase-3 activity, and mitochondrial electrical potential assays. The results showed that exposure of $Ti(OH)_4$ to visible light stimulates the production of ROS and causes dose-dependent necrosis in tumor cells. Also, $Ti(OH)_4$ was capable of inhibiting the proliferation and migration of MB49 in low concentrations. An increase in the mitochondrial membrane potential associated with the accumulation of acid lysosomes and low caspase-3 activity suggests that type II cell death could be initiated by autophagic dysfunction mechanisms associated with high ROS production. In conclusion, the characteristics of $Ti(OH)_4$ make it a potential photosensitizer against bladder cancer.

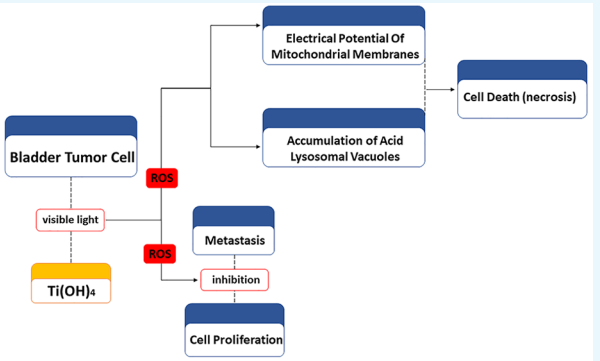

1. INTRODUCTION

Despite recent advances in the prevention and treatment of carcinomas, urothelial bladder cancer (UBC) remains one of the most prevalent and highly recurrent malignant neoplasms.[1] Responsible for 90% of bladder tumors, of which nearly 60 to 80% are limited to regions above the muscular layers, the so-called nonmuscle invasive bladder cancer includes the stages Cis, Ta, and T1.[2] In these subtypes, depending on the risk of progression to the muscle invasive stage, the therapies have been continuously based on the instillation of chemotherapy (mitomycin-C, epirubicin, doxorubicin, pirarubicin, or gemcitabine) or BCG (*bacillus* Calmette-Guérin) and post-transurethral resection of the tumor.[3] Other therapeutic options that are under investigation include laser, photodynamic therapy (PDT), radiation, chemoradiation, immunotherapy, gene therapy, and nanodrug delivery systems using organic or nonorganic nanoparticles.[4] Although chemotherapy, surgery, and immunotherapy have been practiced for decades, some patients with this kind of cancer do not respond to treatment, either due to the severity of the disease or the few available therapy options.[5−7] As a result, the search for more specific therapeutic methods with fewer side effects is of vital importance.

Among the current treatments, PDT is usually less invasive than any surgical option.[8] It is based on the antitumoral action of reactive oxygen species (ROS)[9] produced from the irradiation of photosensitizers (PSs) by a specific wavelength of light in the presence of molecular oxygen.[10,11] Inorganic PS generally has a higher efficiency in converting light to ROS production when compared to organic PS. Still, some studies have also demonstrated that inorganic PS can be targeted to specific tissues, which represents a great advantage in its use for photodynamic therapy.[12]

However, for many malignant tumors, and especially for UBC, the low concentration of oxygen inside the bladder and

Received: December 13, 2021
Accepted: March 9, 2022
Published: May 18, 2022

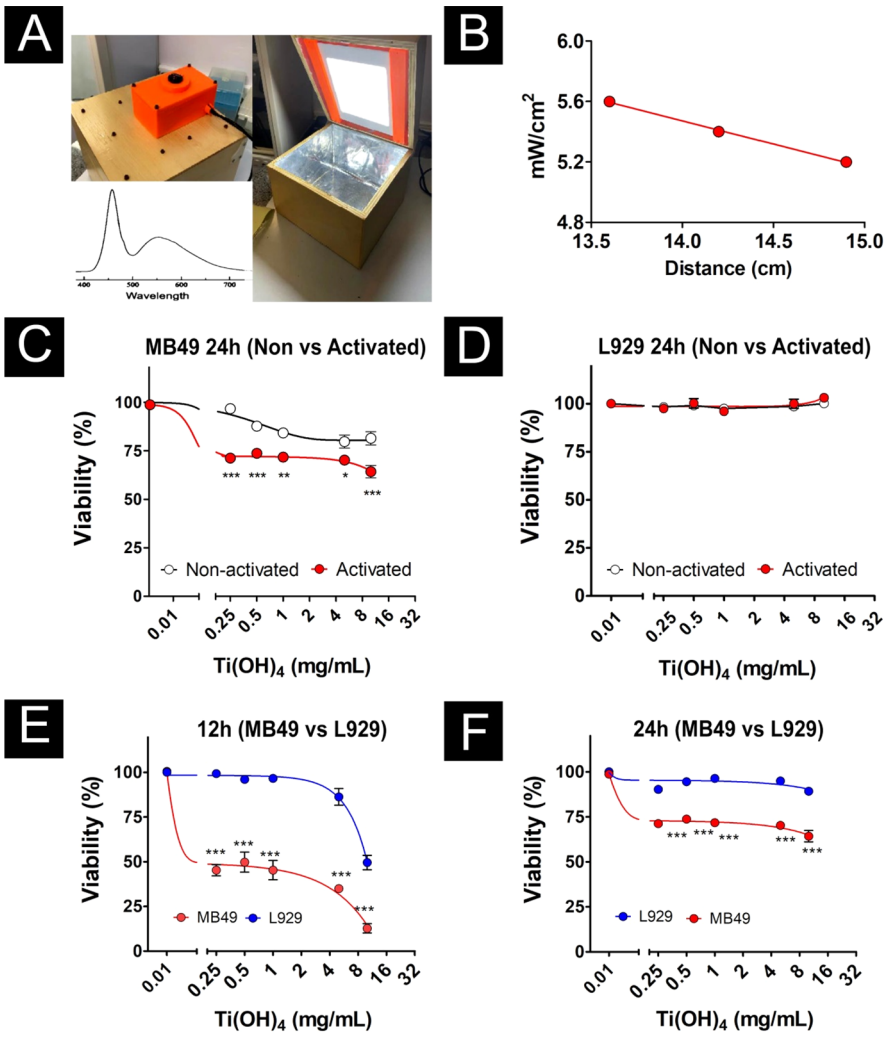

Figure 1. Cytotoxicity assay of nontumor (L929) and bladder tumor (MB49) cells exposed to $Ti(OH)_4$ at the following concentrations: 0.25; 0.5; 1.0; 5.0; and 10.0 mg/mL under different conditions ($n = 4$). (A) System composed of a box (10.5 × 22 × 23 cm) containing a visible light led activated the $Ti(OH)_4$. Image obtained experimentally by the author. (B) Visible light system designed to release about 5.16 mW/cm^2 of energy, distributed by photons with a wavelength between 400 and 750 nm containing two peaks (440 and 550 nm) and a valley at 475 nm. (C) MB49 and (D) L929 exposed to $Ti(OH)_4$ activated or not activated by visible light (1 h) and immediately incubated for 24 h in the dark. (E) Comparison of measuring the cytotoxicity of MB49 and L929 cells when exposed to $Ti(OH)_4$ activated for 1 h under visible light and incubated for 12 h in the dark. (F) Comparison of measuring the cytotoxicity of MB49 and L929 cells when exposed to $Ti(OH)_4$ activated for 1 h under visible light and incubated for 24 h in the dark. Points represent mean values ± the mean standard error (SEM). Statistical differences were established by two-way ANOVA with posthoc analysis using Dunnett's test. Statistically significant values were $p < 0.001$ (***); $p < 0.01$ (**); $p < 0.1$ (*).

in the tumoral microenvironment represents a major barrier for PDT.[7,13] The establishment of hypoxia is a common occurrence in many solid neoplasia such as breast, ovary, head, and neck,[14] including bladder cancer. Turner et al.[15] demonstrated the high expression of a hypoxia marker, the carbonic anhydrase 9 (CA IX), in regions of superficial and invasive bladder tumors. Its expression was most intense on the luminal surface of tumors, indicating the presence of chronic hypoxia. Therefore, innovative PSs for ROS production, which do not depend on the local molecular oxygen concentration, could enhance PDT activity in UBC treatments.

For mammalian cells under physiological conditions, conventional white titanium dioxide (TiO_2) is a nontoxic,[14] stable,[11] and low-cost material[11] that has promising photodynamic properties for cancer treatment.[15] However, like an n-type semiconductor with a high value of a 3.2 eV band gap, TiO_2 tends to produce a larger quantity of ROS when exposed to the smallest wavelengths such as ultraviolet light (254 nm),[16,17] that in function of the mutagenic potential could have its application in PDT restricted.[18] Striving to overcome this limitation, our team developed a new PS with TiO_2 nanoparticles coated with peroxide groups (hereby referred to as $Ti(OH)_4$).[18,19] The covalent binding of these peroxide groups to the surfaces of nanoparticles shifts the band gap to about 2.3 eV,[18,19] hence allowing the $Ti(OH)_4$ to absorb visible light and present equivalent photocatalytic activity when exposed to UV light and about 90% greater activity if compared to common TiO_2.[18] Furthermore, it was demonstrated that the contact of $Ti(OH)_4$ with water can produce OH* radicals even after several photodegradation cycles.[18] Therefore, the use of $Ti(OH)_4$ to treat nonmuscle invasive bladder cancer can be extremely advantageous compared to the PS used thus far.

In this respect, the present study aimed to determine the cytotoxic effects of $Ti(OH)_4$ and identify the main mechanisms of action of PDT based on the use of $Ti(OH)_4$

https://doi.org/10.1021/acsomega.1c07046
ACS Omega 2022, 7, 17563−17574

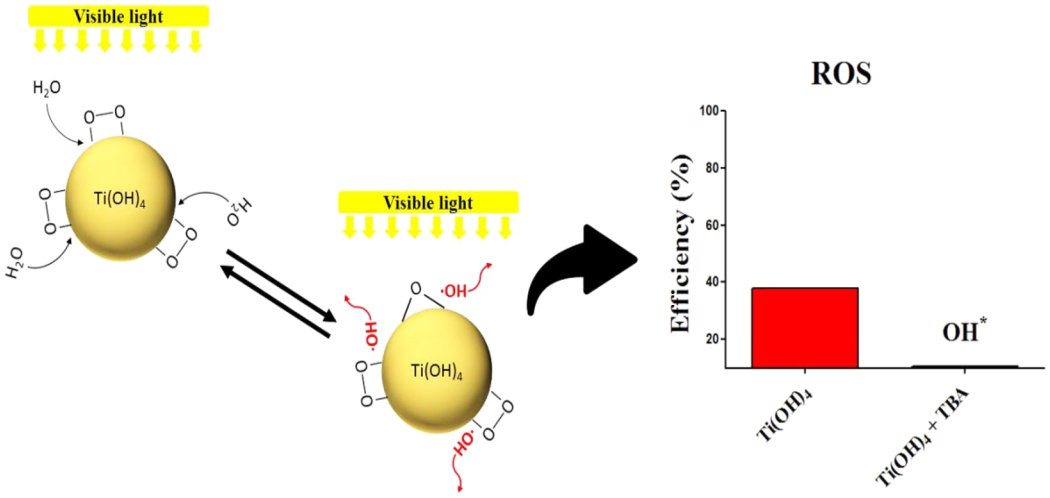

Figure 2. Proposed mechanism for ROS generation by $Ti(OH)_4$. Photocatalytic degradation of RhB of $Ti(OH)_4$ in the presence of TBA under visible light irradiation. The decrease in the bar represents the production and capture of OH* by TBA.

as a PS activated by visible light on a bladder cancer cell line (MB49).

2. RESULTS AND DISCUSSION

2.1. Influence of $Ti(OH)_4$ Contact Time and Activation on MB49 Cell Cytotoxicity. Although PDT is one of the least invasive therapies, it still poses a challenge in treating certain types of malignant neoplasms[20] with low local oxygen availability.[21] The development of a new class of PS that can exert an oxygen-independent antitumor effect could increase the efficacy of PDT.[15,22] The photocatalytic properties of conventional TiO_2 made it widely popular for a variety of applications.[23] Depending on the morphological state, the characteristics of TiO_2 can change the way it interacts with biological molecules, hence, determining its cytotoxic capacity.[23]

In the present study, the cytotoxicity of $Ti(OH)_4$ at different concentrations, whether or not activated by visible light, was determined after 24 h of exposure in bladder tumor cell (MB49) and no-tumor cell lines (L929). Figure 1C,D shows that both cell lines exposed to inactivated $Ti(OH)_4$ preserved their integrity, which was practically equivalent to the untreated group. This can be attributed to the fact that $Ti(OH)_4$ is biocompatible in the absence of light, and only activated $Ti(OH)_4$ can produce high amounts of reactive species after being exposed to light. In addition, a small toxicity was noted for concentrations above 1 mg/mL, but this could have been caused simply by an excess of nanometric material. However, after photoactivation for 1 h (Figure 1A,B) and 24 h of culture, the toxicity of $Ti(OH)_4$ significantly increased over the tumor cell (Figure 1C), regardless of the amount of $Ti(OH)_4$ used. Comparing the time periods for the culture exposed to different amounts of $Ti(OH)_4$ activated by 1 h of visible light (Figure 1E,F), the 12 h culture produced the greatest cytotoxic effect for tumor cells.

The tumor microenvironment is characterized by hypoxia and other byproducts of tumor cell metabolism,[24] which adapt to survive and respond to the increased energy demanded by their high proliferative rate.[24] Highly populated neoplastic areas contain several clones whose sensitivity to oxidative stress varies, generating resistance to hypoxia, which is unusual in healthy cell populations. The results of viability of the MB49 cell line after 24 h of treatment showed higher values in comparison with 12 h. It is likely that clones that survived the initial dose of $Ti(OH)_4$ were able to proliferate and partially recompose the tumor population (Figure 1E).

Moreover, the L929 nontumor line was unaffected by the presence of $Ti(OH)_4$ up to 4 mg/mL after 12 h (Figure 1E) and up to 16 mg/mL after 24 h of exposure (Figure 1F), a distinction that could make $Ti(OH)_4$ advantageous to use in bladder tumor cell selectivity. We chose L929 lineage for this study, because its commonly used as a reference for the assessment of cytotoxicity on tumor cells,[25] besides being very sensitive to reactive oxygen intermediates[26] and having its behavior well established.[27]

Due to the preference for glycolysis to obtain energy, cancer cells, even under aerobic conditions, have a higher metabolism and intrinsic production of ROS than normal cells. Although the antioxidant mechanisms of neoplastic cells are also greater, their antioxidant compensation capacity ends up being completely compromised, making it impossible to adapt to a situation of greater demand. Unlike normal cells, this means that neoplastic cells cannot withstand an additional increase in ROS levels, and therefore, treatments that increase ROS levels end up producing a selective cytotoxic effect on tumor cells.[28] In this sense, the L929 cells, despite being immortalized, do not have an origin from malignant cells, unlike the MB49 lineage, which was obtained by carcinogenic induction. In this case, we can speculate that the L929 strain has a higher threshold of resistance to additional external production of ROS than MB49. It has already been shown that L929 cells have a greater ability to survive under oxidative stress than the cancer lines MDA-MB-231, MCF-7, and T47D.[29]

2.2. Effect of Activated $Ti(OH)_4$ on Intracellular ROS Levels. The successful use of PDT as an anticancer treatment depends on the capacity of the PS to produce ROS and cause intracellular oxidative stress.[7] Usually, oxide photocatalysts just absorb photons to produce electron/hole pairs that will produce ROS from the molecular oxygen available around the nanoparticle.

In the case of $Ti(OH)_4$ instead of molecular O_2, the electron acceptor is the peroxide group bonded to the surface of nanoparticle. Since the photoexcited electron is formed after the absorption of visible light by the peroxide groups on the

https://doi.org/10.1021/acsomega.1c07046
ACS Omega 2022, 7, 17563−17574

surface, the process seems to be similar to the generation of hydroxyl radicals from the reduction of hydrogen peroxide (Figure 2).[18] Since $Ti(OH)_4$ is a mixture of anatase and rutile, the amount of peroxide groups is consumed to produce ROS;[22] however, the material has almost 1 mol of peroxide molecule per gram of nanoparticles, which is a huge amount of oxygen that allows the system to be active during several cycles without a significant decrease of reactivity.[18,19]

Thus, ROS levels of MB49 cells were determined after exposure to $Ti(OH)_4$ activated by visible light (1 h). Probably due to the extremely short half-life of free radicals, most of the ROS responsible for the oxidation of the H2DCF marker are of intrinsic origin. In our case, we can speculate that the ROS detected is more related to the oxidizing activity of internalized $Ti(OH)_4$ than to ROS production in the extracellular environment. Work with nanoparticles has shown that the smaller the nanoparticle, the faster there is the detection of intracellular ROS through DCF oxidation.[30]

Figure 3 shows that the amount of ROS in MB49 cells exposed to a concentration of 0.5 mg/mL of $Ti(OH)_4$ was

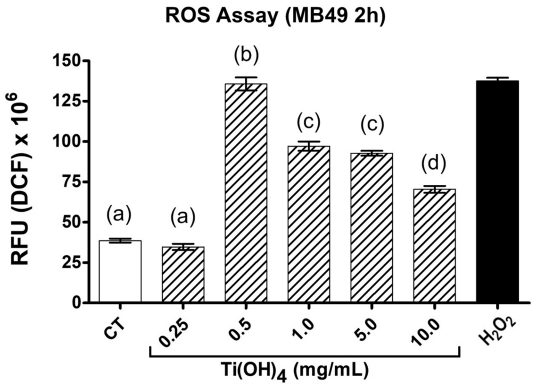

Figure 3. Quantification of intracellular ROS in MB49 cells exposed to $Ti(OH)_4$ activated for 1 h with visible light at the following concentrations: 0.25; 0.5; 1.0; 5.0; 10.0 mg/mL (n = 4). H_2O_2 solution was used as a positive control to induce oxidative stress in cells (10 μmol/L for 30 min of exposure). Cells without any treatment were used as a negative control (CT). Columns represent mean values ± mean standard error (SEM). Statistical differences were established by one-way ANOVA with posthoc analysis using the Tukey's test. Groups with different letters were considered statistically different from each other with $p < 0.01$.

significantly higher compared to the untreated control group. This apparent difference in the relative amounts of ROS can be explained by the specific surface area of nanometric materials.[31−33] Usually, atoms at the surface of nanoparticles exhibit higher energy than those localized on the surface of conventional materials due to the elevated number of unsatisfied chemical bonds.[34,35] However, although the typical particle size of $Ti(OH)_4$ is 5 nm, they can form large agglomerates of up to approximately 800 nm depending on the amount of material added into the system.[18,19,22] This could explain the behavior of the intracellular ROS measurement found in the present study, since the highest concentrations tested can clump together, reducing the apparent catalytic surface area, consequently producing less ROS, as demonstrated in the literature data.[31,34]

2.3. Influence of the Number of Re-exposures to Activated $Ti(OH)_4$ on the Cytotoxicity of MB49 Cells. Most photosensitizers used in PDT are degraded by light.[36,37] This characteristic can be advantageous or disadvantageous in the face of cancer treatment, since the therapy time may not be sufficient for the destruction of the tumor tissue if the photosensitizer undergoes rapid photodegradation during the lighting period.[36−38] This aspect can be corrected by decreasing the light intensity, followed by multiple exposures to PDT.[39]

An analysis of the effect of repeated treatments was performed by exposing MB49 cells to up to three successive repetitions of PDT using different amounts of activated $Ti(OH)_4$, with 12 h of incubation between treatments. Figure 4A shows that for the first or second exposure, the toxicity of

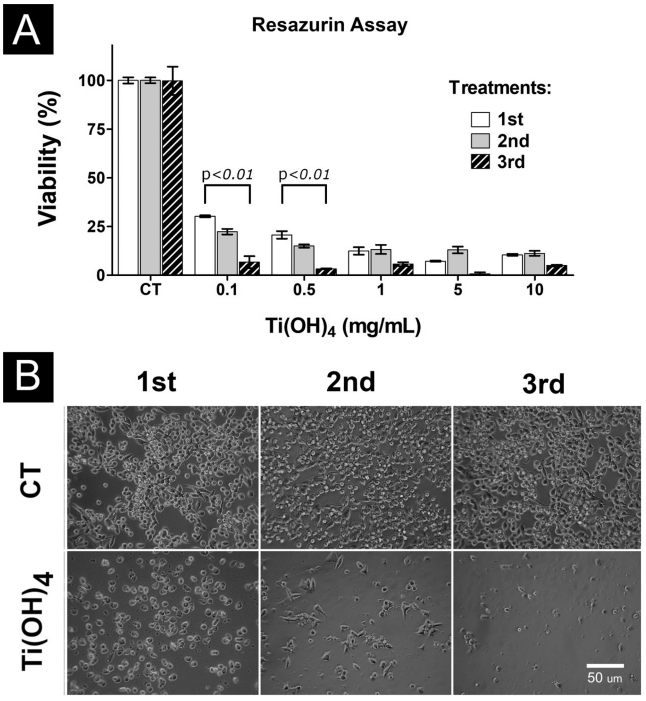

Figure 4. (A) Cytotoxicity assay of MB49 cells exposed to $Ti(OH)_4$ in three re-exposure regimes at the following concentrations: 0.1; 0.5; 1.0; 5.0 and 10.0 mg/mL (n = 4). Treatment I: Exposure of one dose of $Ti(OH)_4$ and quantification of cytotoxicity after 12 h of incubation in the dark. Treatment II: Exposures of two doses of $Ti(OH)_4$ with intermediate 12 h cultivation intervals and quantification of cytotoxicity after 24 h of incubation in the dark. Treatment III: Exposures of three doses of $Ti(OH)_4$ with intermediate 12 h cultivation intervals and quantification of cytotoxicity after 36 h of incubation in the dark. The columns represent the mean values of the groups ± the standard error of the mean (SEM). Statistical differences were established by two-factor ANOVA with posthoc analysis using the Dunnett test. Statistically significant values (***) $p < 0.001$. (B) Representative image of the morphological changes of MB49 cells exposed to a regimen of three subsequent doses of $Ti(OH)_4$ at a concentration of 0.5 mg/mL. Images captured at 20× magnification.

$Ti(OH)_4$ increases in a dose-dependent manner. After the third dose, the toxicity reached the highest value, regardless of the concentration range studied (0.1 to 10 mg/mL). Figure 4B shows a decrease in cell density in comparison with the control group as well as changes in the characteristic phenotype of the cell line as of the first exposure. This result falls in line with the decreased metabolic rates shown in the trial.

2.4. Determining the Type of Cell Death. The type of cell death induced by PDT depends on the cell type, the characteristics of the PS agent (mechanical, optical, electrical,

https://doi.org/10.1021/acsomega.1c07046
ACS Omega 2022, 7, 17563−17574

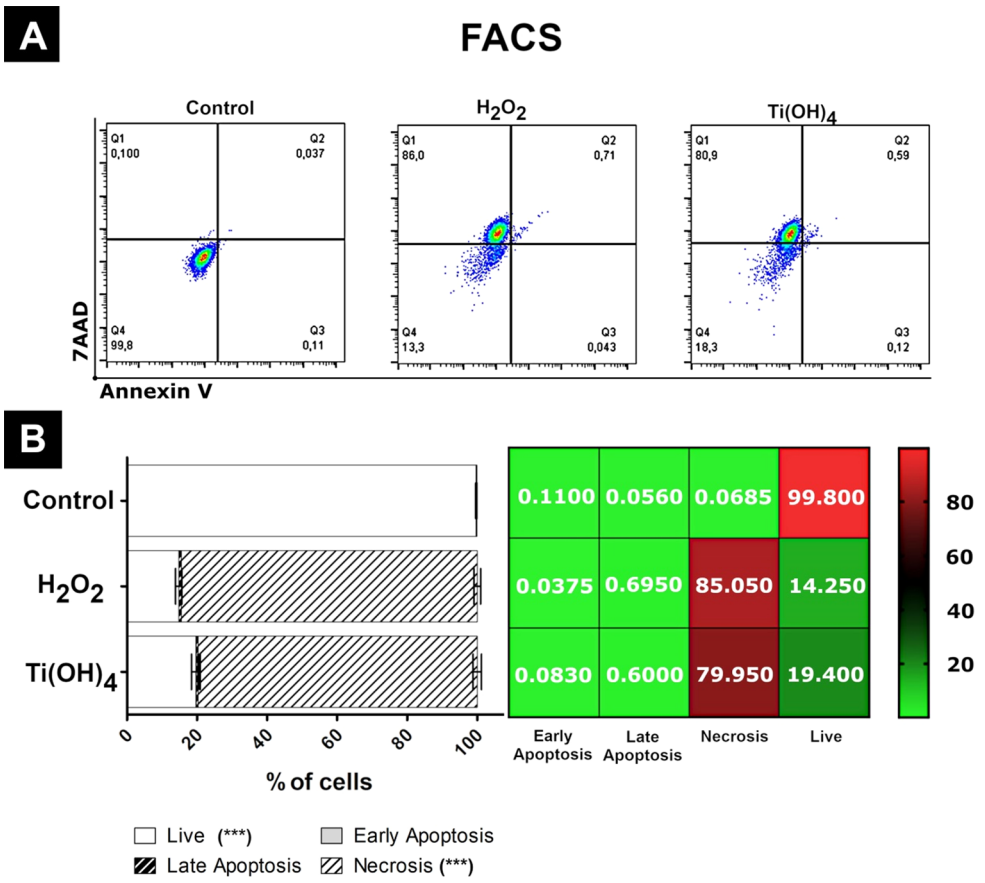

Figure 5. Identification of the type of cell death caused in MB49 cells exposed to three doses of $Ti(OH)_4$ at a concentration of 0.5 mg/mL at 12 h intervals. Untreated control group exposed to H_2O_2 (10 μM for 2 h). Quantification by flow cytometry. (A) Graphs of fluorescent conjugates of 7AAD vs annexin V used to classify subpopulations into: (Q1) cell population in cell death by necrosis; (Q2) population of cells in the final stage of cell death by apoptosis; (Q3) population of cells in the early stages of cell death by apoptosis; (Q4) predominantly viable cell population. (B) Horizontal bar graph showing the significant amounts of live, apoptotic, and necrotic cells present in each analyzed group ± SEM. Statistical differences were established by two-way ANOVA with posthoc analysis using the Bonferroni test. Statistically significant values (***) $p < 0.001$. On the side, a numerical graph shows the predominance of each subpopulation of cells for each analyzed group.

dimensional, morphological, degree of degradability, and surface reactivity), the intracellular location, its concentration, light intensity and excitation wavelength, and amount of molecular oxygen available in the tissues.[8,40] Apoptosis can be induced at lower therapeutic doses[42] by enzymatic activation of the Bcl-2 (Bax/Bcl-2) or the caspase-3 family.[42] On the other hand, higher doses of PDT tend to cause cell death by necrosis, because PDT has a high capacity to produce ROS[43] and can mainly affect the signaling pathways of proteases and calpains.[44] The results of our experiments submitted to flow cytometry showed that the application of three doses of $Ti(OH)_4$ (0.5 mg/mL) predominantly induced cell death by necrosis (80%) in MB49 bladder tumor cells (Figure 5), in addition to a minimal amount of apoptotic cell death (0.68%). This may be directly related to the ability of $Ti(OH)_4$ to produce large amounts of ROS (Figure 2) without requiring molecular oxygen, as in the case of urothelial carcinoma of the bladder. Thus, repetition therapy was able to cause tumor cell necrosis, which can be corroborated by previous studies.[41−43]

Subsequent doses can cause progressive cumulative damage to cell structures and affect clones that may resist oxidative stress better.[25] Other studies found that irreversible damage caused by PDT in tumor cells has been linked to necrotic cell death associated with caspase-independent autophagy,[41,45] resulting from mitochondrial and lysosomal dysfunction.[46,47]

Autophagy is a process commonly known as cellular resistance and survival to stress.[48] It involves the uptake of dysfunctional cytoplasmic proteins and organelles by double-membrane vesicles, which fuse with lysosomes to form autolysosomes, where degradation of cell structures occurs.[40−51] Studies have shown that a high concentration of intracellular ROS can stimulate the direct activation of autophagy.[52,53] Some therapies have used the strategy of autophagic induction in tumor cells[54] to support the response of chemotherapeutic agents.[55] In this case, increased oxidative stress increases intracellular damage and can cause the accumulation of vacuoles that serve to remove the damaged organelles, initiating cell death.[56,57]

Therefore, we compared a possible lysosomal dysfunction with mitochondrial membrane potential and caspase-3 activity to identify the main factor triggering cell death after PDT using $Ti(OH)_4$.

Since mitochondrial functions are mainly affected by increased oxidative stress, the electrical potential of mitochondrial membranes was analyzed by incorporation of rhodamine 123. This is a cationic fluorochrome that is attracted by changes in the level of mitochondrial integrity and can be detected by the increase of cytosolic green fluorescence. In Figure 6A, it can be seen that PDT treatment with $Ti(OH)_4$ in MB49 cells caused a significant difference in electrical

https://doi.org/10.1021/acsomega.1c07046
ACS Omega 2022, 7, 17563−17574

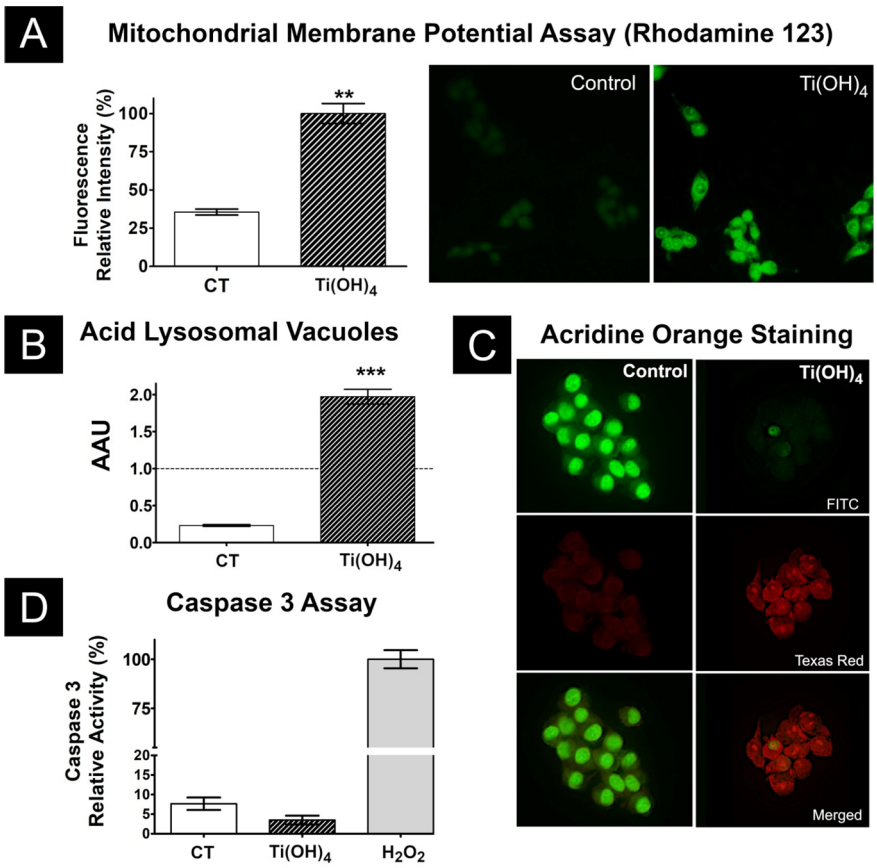

Figure 6. Quantification of acidic lysosomal vacuoles, caspase-3 activation, and mitochondrial electrical potential of MB49 cells exposed to $Ti(OH)_4$ at a concentration of 6 μg/mL activated for 1 h of visible light for 1 and 12 h of incubation in the dark. (A) Qualitative assay of mitochondrial membrane potential: cell images showing the difference in fluorescence intensity produced by exposure of cells to rhodamine 123 in the control group (lower fluorescence intensity) compared to the treated group (higher fluorescence intensity). The opposite bar graph quantitatively compares the mean relative fluorescence intensity ± SEM of the treated group compared to the control group. Statistically significant values (**) $p < 0.01$. Images were acquired at 40× magnification. (B) Neutral red assay of acid lysosomal vacuole quantification: bar graph of intracellular acid vacuole excess unit indices (AUU) calculated by mean ± SEM with data collected from viability assays in relation to neutral red uptake (AAU) > 1 represents type II cell death). Statistically significant values (***) $p < 0.001$. (C) Qualitative assay lysosomal acid vacuoles: images of MB49 cells exposed to the acridine orange fluorophore, showing the morphological differences between the control group that exhibits intense fluorescent activity in the nucleus (FITC filter 525 nm), compared to the groups treated with $Ti(OH)_4$, which exhibits little fluorescent activity in the nucleus, which contains granulations with greater fluorescent intensity in the cytoplasm (Texas Red Filter 650 nm). Images were acquired at 40× magnification. (D) Bar graph comparing the mean caspase-3 enzyme activity ± SEM of the treated group in relation to the control group, which quantified the enzyme activity by applying the EnzChek Caspase-3 kit.

potential, which can be explained by the large amount of ROS produced when $Ti(OH)_4$ was exposed to visible light.

Thus, when analyzing the incorporation of neutral red dye inside MB49 cells, in Figure 6B, it was possible to verify that the correlation between the accumulation of acidic lysosomal vacuoles and cell viability under such conditions, presented values above 1, which is indicative of type II cell death. Likewise, in the analysis of the incorporation of the orange acridine fluorophore, in Figure 6C, it is possible to notice the greater acidification of the cytoplasmic content compared to the control group.[58] Therefore, PDT using $Ti(OH)_4$ causes the accumulation of late lysosomes in bladder cancer cells.

In turn, Figure 6D shows that there was no increase in caspase-3 enzymatic activity in the treated group, which can be interpreted as inhibition of the apoptotic cell death pathway. This observation is in agreement with the literature.[59]

These results suggest that the difference in mitochondrial membrane potential caused by oxidative stress in MB49 cells exposed to $Ti(OH)_4$ could have triggered the accumulation of lysosomal acid vesicles inside the tumor cells. However, large amounts of acidic vesicles are known to lead to type II cell death.[60] Thus, our data suggest that necrotic cell death caused by $Ti(OH)_4$ therapy may be initiated by dysfunctions in the autophagic process. However, more data is needed to support our hypothesis.

2.5. Effect of $Ti(OH)_4$ on the Clonogenic and Migratory Capacity of MB49 Cells. In addition to the cytotoxic capacity of PS as an important and determinant material in photodynamic treatments, strategies against proliferation and metastatic processes have also being targeted in therapeutic studies. For metastasis to be successful, a series of barriers must be overcome: tumor cells must detach from the primary site, reach the blood or lymphatic stream, resist the pressure from blood vessels, extravasate, adapt to the new microenvironment, and resist attacks from the immune system.[61,62] As pointed out by Weng et al.,[63] PDT can reduce the number of tumor cells and prevent them from migrating to adjacent tissues, since the oxidative stress produced during treatment is able to block blood vessels[63−65] and decrease tumor recurrence. Similarly, other studies have shown that

https://doi.org/10.1021/acsomega.1c07046
ACS Omega 2022, 7, 17563−17574

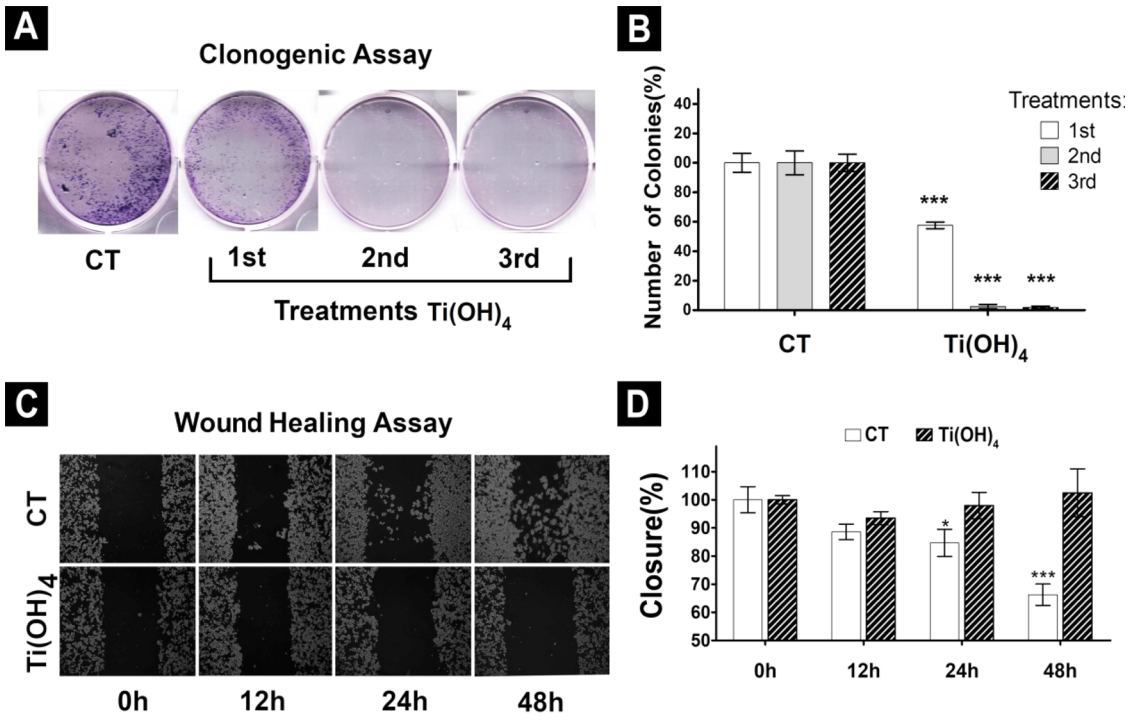

Figure 7. Effect on colony formation and migration of MB49 cells after exposure to three subsequent doses of $Ti(OH)_4$ at a concentration of 6 μg/mL activated by 1 h of light and 12 h of incubation in the dark (n = 4). (A) Qualitative assay colony formation: image corresponding to representative replica of three independent experiments cultivated for 5 days after the respective exposures, showing the inhibition of cell proliferation exposed to a concentration below sublethal. Image obtained experimentally by the author. (B) Quantitative assay colony formation: number of colonies normalized in relation to the control group, statistically showing the differences found in the qualitative assay. The columns represent the mean values of the groups and the standard error of the mean (SEM). Statistical differences were established by a two-way ANOVA test with posthoc analysis using Dunnett's test. Statistically significant values (***) $p < 0.001$. (C) Qualitative assay cell migration: image corresponding to a representative replica of three independent experiments after three subsequent doses and analyzed after 0, 12, 24, and 48 h of exposure, showing the inhibition of cell migration to the determined space when exposed to a concentration below sublethal. Images with 20× magnification. (D) Quantitative assay cell migration: bar graph comparing the mean ± SE SEM measurements of the relative cell free area over the four time intervals. The columns represent the mean values of the groups and the SEM. Statistical differences were established by two-way ANOVA with posthoc analysis using the Dunnett's test. Statistically significant values (***) $p < 0.001$; (*) $p < 0.1$.

autophagy can also play an important role in the metastatic process.[66,67] The formation of autolysosomes can produce focal adhesion complexes that decrease cell motility.[67,68]

As seen in Figure 7, a concentration below the cytotoxic concentration (6 μg/mL), thus incapable of causing MB49 cell death, was used to ensure that only the therapeutic mechanisms of action could be observed. Figure 7A,B shows that only one dose of $Ti(OH)_4$ was not enough to inhibit the proliferative capacity of MB49 cells, given that the tumor cells showed a significant increase in the number of colonies after the postincubation period. However, therapy was able to completely inhibit proliferation and prevent colony formation after exposure to three doses. The clonogenic assay, with its ability to quantify cell growth and cytotoxic or genotoxic effects, has been used as a standard tool to evaluate compounds with antineoplastic action. Our results could indicate that even a cell localized deep within the tumor and submitted to a sublethal dose of the compound could be prevented from colonizing new sites.

Therefore, the cell migration assay assessed the migratory capability of cells toward the chemostatic gradient. As shown in Figure 7C,D, there were no cells in the scratched region after 48 h of re-exposure to three doses of activated $Ti(OH)_4$, whereas grouped cells were observed in the control group after 24 h of culture. In fact, this result may be directly related to the inhibition of the migratory capability of MB49 following PDT, since the variable proliferation was discarded when the FBS was removed from the cell medium. In addition, cells showed no proliferative capacity after re-exposure of three doses of $Ti(OH)_4$, as can also be seen in the cell proliferation assay (Figures 7A,B).

Noninvasive bladder cancers represent 60 to 80% of cases.[2] Even though it has a low rate of invasion and a high chance of patient survival, approximately 30% of these neoplasms tend to progress to invasive muscle and pose a risk of patient survival.[69] Thus, PDT treatment using $Ti(OH)_4$ *in situ* (Cis), noninvasive papillary (Ta), and lamina propria (T1) stages may represent a great perspective in the development of therapy and disease eradication. Following this reasoning, the superficial layers of the bladder are the compartments with the greatest propensity to receive particle instillation and exposure to visible light with less invasiveness, which consequently leads to a more effective treatment.

PDT-based therapy using $Ti(OH)_4$ can employ intravesical installation to concentrate the compound in the tumoral area. We speculate that the increased permeability caused by the loss of umbrella cells during the tumoral development could facilitate the concentration of $Ti(OH)_4$ particles in the affected tissue, potentializing their action over the tumoral area and diminishing the occurrence of off-target effects. While the urothelium is considered impenetrable to most substances

https://doi.org/10.1021/acsomega.1c07046
ACS Omega 2022, 7, 17563−17574

contained in the urine,[70] urothelial cancer cells can internalize more particles than normal umbrella cells.[71]

3. CONCLUSION

In conclusion, $Ti(OH)_4$ can inhibit the proliferation and mobility of MB49 cells at low concentrations and induce death by necrosis at high concentrations. We speculate that the death caused during therapy is possibly activated by mechanisms of mitochondrial and lysosomal dysfunction caused by alterations in the oxidative environment promoted by the high production of ROS.

4. MATERIALS AND METHODS

4.1. Synthesis of $Ti(OH)_4$. $Ti(OH)_4$ was synthesized using the oxidant peroxo method (OPM), a wet-chemical route that allows titanium atoms at the surface to bond to two oxygen atoms, forming a peroxide group, which gives its yellow color.[18] In this method, 3 mL of titanium isopropoxide was added to 40 mL of hydrogen peroxide and heated to 80 °C to form a yellow gel. The gel was dried at 60 °C for 24 h to form a $Ti(OH)_4$ powder. The obtained $Ti(OH)_4$ powder presented an average size of 5 nm. The material presented a thin layer (up to 8%) of peroxide groups in relation to the total mass and a band gap of 2.3 eV, which allowed it to be activated by visible light.[19,22]

4.2. ROS Identification Produced by $Ti(OH)_4$. For the ROS identification, photodegradation of rhodamine B (RhB, P.A., Synth) under visible light was used. In a usual process, 50.0 mg of the $Ti(OH)_4$ was added to 50.0 mL of RhB solution (1×10^{-5} mol L^{-1}). The solution was placed in ultrasound, for greater dispersion of the particles, and left at 30 min in the dark, under constant agitation at 25 °C, for molecular adsorptive balance. After that, the visible light lamps (6×15W, Philips TL-D) were switched on, and an aliquot was removed after 30 min of irradiation. The aliquot was analyzed on an absorption spectrophotometer in the UV−vis region (V-660 spectrophotometer (JASCO)), monitoring the decrease in the characteristic RhB peak at 554 nm. The process was repeated four more times, adding *tert*-butyl alcohol (TBA, 99%, Aldrich) to identify OH*.[72] According to the inhibition of photocatalytic efficiency, it is associated with the reactive species.

4.3. L929 and MB49 Cell Cultures. Murine fibroblast cell line (number cycle: 7, L929-ATCC-CCL-1) and murine transitional carcinoma cell line (MB49 − NCI Thesaurus Code: C25823), courtesy of Dr. Yi Lou (University of Iowa), were cultivated in Dulbecco's Modified Eagle Medium (DMEM) supplemented with a high glucose concentration of L-glutamine (2 mmol/L, Cultilab, Campinas, Brazil), 10% fetal bovine serum (FBS, Cultilab), and 1% penicillin + streptomycin (Vitrocell Embriolife, Campinas, Brazil) (i.e., complete medium). Cells were maintained in a humid incubator at 37 °C and 5% CO_2.

4.4. Cytotoxicity of $Ti(OH)_4$ in the Absence and Presence of Visible Light. L929 and MB49 cells were seeded in 96-well culture plates (Corning, NY, USA) at a concentration of 1×10^5 cells/well in a complete DMEM culture medium and allowed to adhere. Cells were exposed to a suspension of $Ti(OH)_4$ at the following concentrations: 10.0; 5.0; 1.0; 0.5; and 0.25 mg/mL in conjunction with a negative control composed of untreated cells. One of the plates containing cells and $Ti(OH)_4$ was kept incubated in the dark for the entire experimental period to investigate the action of inactivated $Ti(OH)_4$. A second plate was placed for 1 h in a box ($10.5 \times 22 \times 23$ cm) containing a visible light source designed to activate the $Ti(OH)_4$ (12 W power white LED, 1170 lm, 6000k color temperature at an irradiation distance of 15 cm), which released about 5.16 mW/cm^2 of energy in the cell culture line as measured by the equipment (PM20HC - ThorLabs, USA). This energy was distributed by photons with a wavelength between 400 and 750 nm, containing two peaks (440 and 550 nm) and a valley at 475 nm (Figure 1). Since cell culture plates are made of plastic with no reflectance capability, they were placed in a closed box with the side walls and bottom covered with reflective material.

After this procedure, both plates were incubated in the dark for 12 and 24 h, and the resulting cells were washed with phosphate-buffered saline (PBS 1×). A cell toxicity test was performed by adding 200 μL/well of resazurin (70 μmol/L solution, Sigma-Aldrich, USA) in PBS 1×. Absorbance was measured in a spectrophotometer with wavelengths of 570 and 600 nm.[73]

4.5. Intracellular Reactive Oxygen Species Quantification Assay. MB49 cells were seeded in 96-well black wall plates (Corning, NY, USA) at a concentration of 1×10^5 cells/well and exposed to a complete medium with $Ti(OH)_4$ activated for 1 h with visible light. A solution of 10 μmol/L of H_2O_2 was used (30 min of exposure) as a positive control to induce oxidative stress in the cells. Cells without any treatment were used as a negative control. After the exposure period, the cells were washed with PBS (1×) and labeled with 30 μL of a 100 μmol/L solution of 2′,7′-dichlorofluorescein diacetate (DCF-DA) (Sigma-Aldrich, USA). Fluorescence readings were taken using the Spectra Max i3 (Molecular Devices) with 485−530 nm excitation.[74]

4.6. Cytotoxicity of MB49 Cells in Relation to Re-Exposure to Activated $Ti(OH)_4$. MB49 cells were subjected to three exposure designs (one, two, or three doses) for the following different concentrations to assess the effects of re-exposure to activated $Ti(OH)_4$ (1 h): 10.0; 5.0; 1.0; 0.5; 0.1 mg/mL in accordance with the following protocols: DESIGN 1: exposure of one dose and quantification of toxicity after 12 h; DESIGN 2: exposures of two doses with intermediate 12 h cultivation intervals and quantification of toxicity after 24 h; DESIGN 3: exposures of three doses with intermediate cultivation intervals of 12 h and quantification of toxicity after 36 h. Cells were washed with PBS (1×) before each re-exposure, and a newly activated composite medium was reintroduced.

4.7. Effect on Clonogenic Capacity of MB49 Cells in Relation to Re-Exposure to Activated $Ti(OH)_4$. MB49 cells were seeded in six-well plates (Corning, NY, USA) at a concentration of 300 cells/well under the same incubation conditions as the experiment described in Section 4.6, except that the cells were washed with PBS (1×), and kept in complete DMEM culture medium for 5 days after the respective periods of exposure to $Ti(OH)_4$. In this assay, a noncytotoxic concentration (6.0 μg/mL), which inhibited proliferation without causing defined cell death, was chosen to analyze the mechanism of inhibiting colony formation. This procedure was optimized in previous tests (data not shown). Resulting cells were fixed in absolute methanol and stained with 0.1% crystal violet (Corning, NY, USA). The digitized images of the colonies were analyzed using the ImageJ software.[75]

https://doi.org/10.1021/acsomega.1c07046
ACS Omega 2022, 7, 17563−17574

4.8. Effect of Activated $Ti(OH)_4$ on Cell Migration Assessed by the Risk Closure Assay (Wound Healing Assay). MB49 cells were seeded in 12-well plates (Corning, NY, USA) at a concentration of 5×10^5 cells/well. The cells were maintained for 24 h in DMEM supplemented with 1% FBS to ensure basal activity levels. A scratch was performed in the central portion of the well with a 200 μL tip and a sterile ruler. Next, the wells were carefully washed with PBS (1×) to remove cell debris from the scratched area. Cells were treated with three doses of $Ti(OH)_4$ at a concentration of 6.0 μg/mL, just as described in Section 4.6. Images were captured after 12, 24, and 48 h with an inverted microscope coupled with an image capture system. The area of closure by cell migration was measured with the ImageJ software, and the percentage of closure was calculated as described below.[76,77]

$$(\%)\text{stripe closing} = \frac{(A_{t=0h} - A_{t=\Delta h})}{(A_{t=0h})} \times (100\%)$$

where $A_{t=0h}$ is the measurement of the streaked area immediately after determination and $A_{t=\Delta h}$ is the streaked area measured at 12, 24, or 48 h after incubation.

4.9. Characterization of Cell Death after Treatment with Activated $Ti(OH)_4$. *4.9.1. Identification of the Type of Cell Death.* MB49 cells were seeded in 12-well plates (Corning, NY, USA) and treated with activated $Ti(OH)_4$ (0.5 mg/mL). An aliquot of 10 μmol/L of H_2O_2 (2 h exposure) was used as a positive control, and an untreated culture was used as a negative control. After applying the three-dose $Ti(OH)_4$ treatment described in Section 4.6, cells were centrifuged at 320*g* for 10 min at 4 °C, carefully washed with PBS (1×), and suspended in 200 μL of binding buffer. Next, they were detached from the plate and transferred to microtubes, which were incubated at room temperature with 1 μL of annexin V and 1 μL of the 7-AAD Detection Kit (BD Biosciences) for 15 min in the dark. Samples were centrifuged at 320*g* for 10 min at 4 °C, and the dye solutions were carefully discarded. Cells were suspended in 300 μL of 1× binding buffer. The FACS was performed by a BD Accuri C7 cytometer (BD Biosciences), and biparametric dot plots were analyzed using a FCS Express software program (De Novo Software).[78]

4.9.2. Lysosomal Quantification. To quantify the accumulation of lysosomal acidic vesicles, MB49 cells were seeded in 96-well plates at a concentration of 1×10^5 cell/mL. After exposure with one dose of $Ti(OH)_4$ at a concentration of 6.0 μg/mL for 12 h, cells were washed with PBS (1×) and exposed to a neutral red solution (30 μg/mL of neutral red in 1% DMEM FBS) (Sigma-Aldrich, USA) at 37 °C and 5% CO_2 for 2 h. Cells were washed with PBS (1×), and the neutral red retained inside the lysosomes was eluted in a solution of ethanol (50% v/v) and acetic acid (1% v/v) for 10 min. Measurement of the lysosomotropic incorporation was estimated using a spectrophotometer with a wavelength range from 540 to 800 nm. Absorption values were converted into relative indices using the positive (10 μmol/L H_2O_2 for 30 min) and negative (culture medium) controls. The estimate of type II cell death was obtained by applying the unit index of acidic vesicle excess (AAU> 1), calculated by dividing the mean relative neutral red retention by the relative cell viability quantified by the resazurin assay, performed in parallel.[79]

Qualitatively, the excess of late lysosomes was verified by labeling the orange acridine fluorophore, since the cytoplasmic acidity transforms the green fluorophore into red. Therefore, the process was performed by seeding MB49 cells in coverslips placed on six-well plates at a concentration of 1×10^4 cells/mL, followed by treatment with one dose of $Ti(OH)_4$ at a concentration of 6.0 μg/mL. A solution of 10 μmol/L of H_2O_2 (2 h of exposure) was used as a positive control, and an untreated culture was used as a negative control. After the exposure period, cells were washed with PBS (1×) and stained with 50 μL (1 mg/mL) of a acridine orange fluorophore (Sigma-Aldrich, USA) for 15 min in the absence of light. Cells were washed, and coverslips were assembled on slides for observation under a fluorescence microscope. Images were captured at 40× magnification.[80]

4.9.3. Quantification of Mitochondrial Electrical Potential. MB49 cells (1×10^4 cells/mL) were seeded in coverslips placed on six-well plates and treated with one dose of $Ti(OH)_4$ at a concentration of 6.0 μg/mL. Cells were washed with DMEM, and 50 μL of rhodamine 123 solution (1 mg/mL in ethanol, Sigma-Aldrich, USA) was added for 15 min in the dark at 37 °C. Afterward, cells were washed with PBS (1×), and coverslips were assembled on slides for observation under a fluorescence microscope. Images were captured at 40× magnification and analyzed with an ImageJ software program.[81]

4.9.4. Caspase-3 Enzyme Activity. MB49 cells were seeded in six-well plates at a concentration of 1×10^5 cells/mL and treated with one dose of $Ti(OH)_4$ at a concentration of 6 μg/mL. The assay for quantifying caspase enzymatic activity was performed using the EnzChekCaspase-3 kit (E-13183-Molecular Probe, Leiden, The Netherlands), following the protocol according to the manufacturer's guidelines. Fluorescence measurements were performed using the Spectra-Max i3 (Molecular Devices) with 342/441 nm excitation/emission wavelengths.[82]

4.10. Statistical Analysis. Quantitative data were analyzed with one- and two-way ANOVA statistical tests with posthoc tests by either the Dunnett or Tukey tests. The results were expressed as a standard error of the mean (SEM). In cases where the results did not follow normality, the data were analyzed using the Kruskal−Wallis analysis of variance tes , and the Dunn test for two-by-two comparisons. The Prism software program version 5.0 (GraphPad Software), was used to perform the statistical analysis, and $p < 0.05$ values were considered significant.

AUTHOR INFORMATION

Corresponding Author

Thaiane Robeldo − *Laboratory of Applied Immunology, Federal University of São Carlos (UFSCar), São Carlos, São Paulo 13565-905, Brazil; CDMF, LIEC, Chemistry Department of the Federal University of São Carlos (UFSCar), São Carlos, São Paulo 13565-905, Brazil;* orcid.org/0000-0002-7262-4969; Phone: +55(19) 984308868; Email: tharobeldo@gmail.com

Authors

Lucas S. Ribeiro − *CDMF, LIEC, Chemistry Department of the Federal University of São Carlos (UFSCar), São Carlos, São Paulo 13565-905, Brazil;* orcid.org/0000-0001-6314-0076

Lida Manrique − *Laboratory of Applied Immunology, Federal University of São Carlos (UFSCar), São Carlos, São Paulo 13565-905, Brazil*

https://doi.org/10.1021/acsomega.1c07046
ACS Omega 2022, 7, 17563−17574

Andressa Mayumi Kubo − *CDMF, LIEC, Chemistry Department of the Federal University of São Carlos (UFSCar), São Carlos, São Paulo 13565-905, Brazil*
Elson Longo − *CDMF, LIEC, Chemistry Department of the Federal University of São Carlos (UFSCar), São Carlos, São Paulo 13565-905, Brazil;* orcid.org/0000-0001-8062-7791
Emerson Rodrigues Camargo − *CDMF, LIEC, Chemistry Department of the Federal University of São Carlos (UFSCar), São Carlos, São Paulo 13565-905, Brazil*
Ricardo Carneiro Borra − *Laboratory of Applied Immunology, Federal University of São Carlos (UFSCar), São Carlos, São Paulo 13565-905, Brazil*

Complete contact information is available at: https://pubs.acs.org/10.1021/acsomega.1c07046

Notes

The authors declare no competing financial interest.

■ ACKNOWLEDGMENTS

Funding: The present study was supported by the Coordenação de Aperfeiçoamento de Pessoal de Nível Superior − Brasil (CAPES - www.capes.gov.br/) [Funding Code 001], Fundação e Amparo à Pesquisa do Estado de São Paulo (FAPESP - www.fapesp.br/) [grant numbers: 2013/00789-2, 2017/24832-6, and CEPID 2013/07296-2], and Conselho Nacional de Desenvolvimento Científico e Tecnológico (CNPq - www.gov.br/cnpq) [Funding Code: 309711/2019-3]. The fund grantors had no role in the study design, data collection and analysis, decision to publish, or preparation of the manuscript.

■ REFERENCES

(1) Lenis, A. T.; Lec, P. M.; Chamie, K.; Mshs, M. D. Bladder Cancer: A Review. *JAMA* **2020**, *324* (19), 1980−1991.
(2) Knowles, M. A.; Hurst, C. D. Molecular Biology of Bladder Cancer: New Insights into Pathogenesis and Clinical Diversity. *Nat. Rev. Cancer* **2015**, *15* (1), 25−41.
(3) Bhindi, B.; Kool, R.; Kulkarni, G. S.; Siemens, D. R.; Aprikian, A. G.; Breau, R. H.; Brimo, F.; Fairey, A.; French, C.; Hanna, N.; Izawa, J. I.; Lacombe, L.; McPherson, V.; Rendon, R. A.; Shayegan, B.; So, A. I.; Zlotta, A. R.; Black, P. C.; Kassouf, W. Canadian Urological Association Guideline on the Management of Non-Muscle-Invasive Bladder Cancer - Abridged Version. *Can. Urol. Assoc. J.* **2021**, *15* (8), 230−239.
(4) Jain, P.; Kathuria, H.; Momin, M. Clinical Therapies and Nano Drug Delivery Systems for Urinary Bladder Cancer. *Pharmacol. Ther.* **2021**, *226*, 107871.
(5) Richters, A.; Aben, K. K. H.; Kiemeney, L. A. L. M. The Global Burden of Urinary Bladder Cancer: An Update. *World J. Urol.* **2020**, *38* (8), 1895−1904.
(6) Dinney, C. P. N.; McConkey, D. J.; Millikan, R. E.; Wu, X.; Bar-Eli, M.; Adam, L.; Kamat, A. M.; Siefker-Radtke, A. O.; Tuziak, T.; Sabichi, A. L.; Grossman, H. B.; Benedict, W. F.; Czerniak, B. Focus on Bladder Cancer. *Cancer Cell* **2004**, *6* (2), 111−116.
(7) Railkar, R.; Agarwal, P. K. Photodynamic Therapy in the Treatment of Bladder Cancer: Past Challenges and Current Innovations. *Eur. Urol. Focus* **2018**, *4* (4), 509−511.
(8) Tomlinson, B.; Lin, T.; Dall'Era, M.; Pan, C.-X. Nanotechnology in Bladder Cancer: Current State of Development and Clinical Practice. *Nanomedicine (Lond)* **2015**, *10* (7), 1189−1201.
(9) Song, C.; Xu, W.; Wu, H.; Wang, X.; Gong, Q.; Liu, C.; Liu, J.; Zhou, L. Photodynamic Therapy Induces Autophagy-Mediated Cell Death in Human Colorectal Cancer Cells via Activation of the ROS/JNK Signaling Pathway. *Cell Death Dis.* **2020**, *11* (10), 938.
(10) Calixto, G. M. F.; Bernegossi, J.; De Freitas, L. M.; Fontana, C. R.; Chorilli, M. Nanotechnology-based drug delivery systems for photodynamic therapy of cancer: A review. *Molecules* **2016**, *21*, 342. Calixto, G. M. F.; Bernegossi, J.; de Freitas, L. M.; Fontana, C. R.; Chorilli, M. Nanotechnology-Based Drug Delivery Systems for Photodynamic Therapy of Cancer: A Review. *Molecules* **2016**, *21* (3), 342.
(11) Wu, S.; Wang, F.; Li, Q.; Wang, J.; Zhou, Y.; Duan, N.; Niazi, S.; Wang, Z. Photocatalysis and Degradation Products Identification of Deoxynivalenol in Wheat Using Upconversion Nanoparticles@TiO2 Composite. *Food. Chem.* **2020**, *323*, 126823.
(12) Zhou, Z.; Zhang, L.; Zhang, Z.; Liu, Z. Advances in Photosensitizer-Related Design for Photodynamic Therapy. *Asian J. Pharm. Sci.* **2021**, *16* (6), 668−686.
(13) Liang, C.; Zhang, X.; Yang, M.; Wang, W.; Chen, P.; Dong, X. Remodeling Tumor Microenvironment by Multifunctional Nano-assemblies for Enhanced Photodynamic Cancer Therapy. *ACS Mater. Lett.* **2020**, *2* (10), 1268−1286.
(14) Wykoff, C. C.; Beasley, N. J.; Watson, P. H.; Turner, K. J.; Pastorek, J.; Sibtain, A.; Wilson, G. D.; Turley, H.; Talks, K. L.; Maxwell, P. H.; Pugh, C. W.; Ratcliffe, P. J.; Harris, A. L. Hypoxia-Inducible Expression of Tumor-Associated Carbonic Anhydrases. *Cancer Res.* **2000**, *60* (24), 7075−7083.
(15) Turner, K. J.; Crew, J. P.; Wykoff, C. C.; Watson, P. H.; Poulsom, R.; Pastorek, J.; Ratcliffe, P. J.; Cranston, D.; Harris, A. L. The Hypoxia-Inducible Genes VEGF and CA9 Are Differentially Regulated in Superficial vs Invasive Bladder Cancer. *Br. J. Cancer* **2002**, *86* (8), 1276−1282.
(16) Fabian, E.; Landsiedel, R.; Ma-Hock, L.; Wiench, K.; Wohlleben, W.; van Ravenzwaay, B. Tissue Distribution and Toxicity of Intravenously Administered Titanium Dioxide Nanoparticles in Rats. *Arch. Toxicol.* **2008**, *82* (3), 151−157.
(17) Moosavi, M. A.; Sharifi, M.; Ghafary, S. M.; Mohammadalipour, Z.; Khataee, A.; Rahmati, M.; Hajjaran, S.; Łos, M. J.; Klonisch, T.; Ghavami, S. Photodynamic N-TiO2 Nanoparticle Treatment Induces Controlled ROS-Mediated Autophagy and Terminal Differentiation of Leukemia Cells. *Sci. Rep.* **2016**, *6*, 34413.
(18) Nogueira, A. E.; Ribeiro, L. S.; Gorup, L. F.; Silva, G. T. S. T.; Silva, F. F. B.; Ribeiro, C.; Camargo, E. R. New Approach of the Oxidant Peroxo Method (OPM) Route to Obtain Ti(OH)4 Nanoparticles with High Photocatalytic Activity under Visible Radiation. *Int. J. Photoenergy* **2018**, *2018*, 6098302.
(19) Ribeiro, L. S.; Nogueira, A. E.; Aquino, J. M.; Camargo, E. R. A New Strategy to Obtain Nano-Scale Particles of Lithium Titanate (Li4Ti5O12) by the Oxidant Peroxo Method (OPM). *Ceram. Int.* **2019**, *45* (18), 23917−23923.
(20) Geso, M. Nanoparticle Augmented Radiation Treatment Decreases Cancer Cell Proliferation. *Nanomedicine* **2013**, *9* (2), 302−303.
(21) You, D. G.; Deepagan, V. G.; Um, W.; Jeon, S.; Son, S.; Chang, H.; Yoon, H. I.; Cho, Y. W.; Swierczewska, M.; Lee, S.; Pomper, M. G.; Kwon, I. C.; Kim, K.; Park, J. H. ROS-Generating TiO2 Nanoparticles for Non-Invasive Sonodynamic Therapy of Cancer. *Sci. Rep.* **2016**, *6*, 23200.
(22) Francatto, P.; Souza Neto, F. N.; Nogueira, A. E.; Kubo, A. M.; Ribeiro, L. S.; Gonçalves, L. P.; Gorup, L. F.; Leite, E. R.; Camargo, E. R. Enhanced Reactivity of Peroxo-Modified Surface of Titanium Dioxide Nanoparticles Used to Synthesize Ultrafine Bismuth Titanate Powders at Lower Temperatures. *Ceram. Int.* **2016**, *42* (14), 15767−15772.
(23) Çeşmeli, S.; Biray Avci, C. Application of Titanium Dioxide (TiO2) Nanoparticles in Cancer Therapies. *J. Drug Targeting* **2019**, *27* (7), 762−766.
(24) Netea-Maier, R. T.; Smit, J. W. A.; Netea, M. G. Metabolic Changes in Tumor Cells and Tumor-Associated Macrophages: A Mutual Relationship. *Cancer Lett.* **2018**, *413*, 102−109.
(25) Ivankovic, S.; Stojkovic, R.; Jukic, M.; Milos, M.; Milos, M.; Jurin, M. The Antitumor Activity of Thymoquinone and Thymohydroquinone in Vitro and in Vivo. *Exp. Oncol.* **2006**, *28* (3), 220−224.

(26) Goossens, V.; Grooten, J.; De Vos, K.; Fiers, W. Direct Evidence for Tumor Necrosis Factor-Induced Mitochondrial Reactive Oxygen Intermediates and Their Involvement in Cytotoxicity. *Proc. Natl. Acad. Sci. U S A* **1995**, *92* (18), 8115−8119.
(27) Humphreys, D. T.; Wilson, M. R. Modes of L929 Cell Death Induced by TNF-Alpha and Other Cytotoxic Agents. *Cytokine* **1999**, *11* (10), 773−782.
(28) Liu, J.; Wang, Z. Increased Oxidative Stress as a Selective Anticancer Therapy. *Oxid. Med. Cell. Longevity* **2015**, *2015*, 294303.
(29) Salehi, F.; Behboudi, H.; Kavoosi, G.; Ardestani, S. K. Oxidative DNA Damage Induced by ROS-Modulating Agents with the Ability to Target DNA: A Comparison of the Biological Characteristics of Citrus Pectin and Apple Pectin. *Sci. Rep.* **2018**, *8* (1), 13902.
(30) Onodera, A.; Nishiumi, F.; Kakiguchi, K.; Tanaka, A.; Tanabe, N.; Honma, A.; Yayama, K.; Yoshioka, Y.; Nakahira, K.; Yonemura, S.; Yanagihara, I.; Tsutsumi, Y.; Kawai, Y. Short-Term Changes in Intracellular ROS Localisation after the Silver Nanoparticles Exposure Depending on Particle Size. *Toxicol. Rep.* **2015**, *2*, 574−579.
(31) Lanone, S.; Boczkowski, J. Biomedical Applications and Potential Health Risks of Nanomaterials: Molecular Mechanisms. *Curr. Mol. Med.* **2006**, *6* (6), 651−663.
(32) Wilson, M. R.; Lightbody, J. H.; Donaldson, K.; Sales, J.; Stone, V. Interactions between Ultrafine Particles and Transition Metals in Vivo and in Vitro. *Toxicol. Appl. Pharmacol.* **2002**, *184* (3), 172−179.
(33) Sioutas, C.; Delfino, R. J.; Singh, M. Exposure Assessment for Atmospheric Ultrafine Particles (UFPs) and Implications in Epidemiologic Research. *Environ. Health Perspect.* **2005**, *113* (8), 947−955.
(34) Abdal Dayem, A. A.; Hossain, M. K.; Lee, S. B.; Kim, K.; Saha, S. K.; Yang, G.-M.; Choi, H. Y.; Cho, S.-G. The Role of Reactive Oxygen Species (ROS) in the Biological Activities of Metallic Nanoparticles. *Int. J. Mol. Sci.* **2017**, *18* (1), 120.
(35) Fan, J.; Yin, J.-J.; Ning, B.; Wu, X.; Hu, Y.; Ferrari, M.; Anderson, G. J.; Wei, J.; Zhao, Y.; Nie, G. Direct Evidence for Catalase and Peroxidase Activities of Ferritin-Platinum Nanoparticles. *Biomaterials* **2011**, *32* (6), 1611−1618.
(36) Bonnett, R.; Martinez, G. Photobleaching of Sensitisers Used in Photodynamic Therapy. *Tetrahedron.* **2001**, *57*, 9513−9547.
(37) Stratonnikov, A. A.; Meerovich, G. A.; Loschenov, V. Photobleaching of Photosensitizers Applied for Photodynamic Therapy. *BiOS 2000 The International Symposium on Biomedical Optics* **2000**, 81.
(38) Rotomskis, R.; Streckyte, G.; Bagdonas, S. Phototransformations of Sensitizers 1. Significance of the Nature of the Sensitizer in the Photobleaching Process and Photoproduct Formation in Aqueous Solution. *J. Photochem., B* **1997**, *39* (2), 167−171.
(39) Hadjur, C.; Lange, N.; Rebstein, J.; Monnier, P.; van den Bergh, H.; Wagnières, G. Spectroscopic Studies of Photobleaching and Photoproduct Formation of Meta(Tetrahydroxyphenyl)Chlorin (m-THPC) Used in Photodynamic Therapy. The Production of Singlet Oxygen by m-THPC. *J. Photochem., B* **1998**, *45* (2), 170−178.
(40) Sai, D. L.; Lee, J.; Nguyen, D. L.; Kim, Y. P. Tailoring photosensitive ROS for advanced photodynamic therapy. *Exp. Mol. Med.* **2021**, *53*, 495.
(41) Mroz, P.; Yaroslavsky, A.; Kharkwal, G. B.; Hamblin, M. R. Cell Death Pathways in Photodynamic Therapy of Cancer. *Cancers (Basel)* **2011**, *3* (2), 2516−2539.
(42) Perillo, B.; Di Donato, M.; Pezone, A.; Di Zazzo, E.; Giovannelli, P.; Galasso, G.; Castoria, G.; Migliaccio, A. ROS in Cancer Therapy: The Bright Side of the Moon. *Exp. Mol. Med.* **2020**, *52* (2), 192−203.
(43) Almeida, R. D.; Manadas, B. J.; Carvalho, A. P.; Duarte, C. B. Intracellular Signaling Mechanisms in Photodynamic Therapy. *Biochim. Biophys. Acta, Rev. Cancer* **2004**, *1704* (2), 59−86.
(44) Buytaert, E.; Dewaele, M.; Agostinis, P. Molecular Effectors of Multiple Cell Death Pathways Initiated by Photodynamic Therapy. *Biochim. Biophys. Acta, Rev. Cancer* **2007**, *1776* (1), 86−107.
(45) Buytaert, E.; Callewaert, G.; Hendrickx, N.; Scorrano, L.; Hartmann, D.; Missiaen, L.; Vandenheede, J. R.; Heirman, I.; Grooten, J.; Agostinis, P. Role of Endoplasmic Reticulum Depletion and Multidomain Proapoptotic BAX and BAK Proteins in Shaping Cell Death after Hypericin-Mediated Photodynamic Therapy. *FASEB J.* **2006**, *20* (6), 756−758.
(46) Martins, W. K.; Costa, É. T.; Cruz, M. C.; Stolf, B. S.; Miotto, R.; Cordeiro, R. M.; Baptista, M. S. Parallel Damage in Mitochondrial and Lysosomal Compartments Promotes Efficient Cell Death with Autophagy: The Case of the Pentacyclic Triterpenoids. *Sci. Rep.* **2015**, *5*, 12425.
(47) Martins, W. K.; Santos, N. F.; Rocha, C. de S.; Bacellar, I. O. L.; Tsubone, T. M.; Viotto, A. C.; Matsukuma, A. Y.; Abrantes, A. B. de P.; Siani, P.; Dias, L. G.; Baptista, M. S. Parallel Damage in Mitochondria and Lysosomes Is an Efficient Way to Photoinduce Cell Death. *Autophagy* **2019**, *15* (2), 259−279.
(48) Lin, J.; Huang, Z.; Wu, H.; Zhou, W.; Jin, P.; Wei, P.; Zhang, Y.; Zheng, F.; Zhang, J.; Xu, J.; Hu, Y.; Wang, Y.; Li, Y.; Gu, N.; Wen, L. Inhibition of Autophagy Enhances the Anticancer Activity of Silver Nanoparticles. *Autophagy* **2014**, *10* (11), 2006−2020.
(49) Baehrecke, E.; Autophagy, H. Dual Roles in Life and Death? *Nat. Rev. Mol. Cell. Biol.* **2005**, *6* (6), 505−510.
(50) Levine, B.; Yuan, J. Autophagy in Cell Death: An Innocent Convict? *J. Clin. Invest.* **2005**, *115* (10), 2679−2688.
(51) Gozuacik, D.; Kimchi, A. Autophagy as a Cell Death and Tumor Suppressor Mechanism. *Oncogene* **2004**, *23* (16), 2891−2906.
(52) Stern, S. T.; Adiseshaiah, P. P.; Crist, R. M. Autophagy and Lysosomal Dysfunction as Emerging Mechanisms of Nanomaterial Toxicity. *Part. Fibre Toxicol.* **2012**, *9*, 20.
(53) Amaravadi, R. K.; Thompson, C. B. The Roles of Therapy-Induced Autophagy and Necrosis in Cancer Treatment. *Clin. Cancer Res.* **2007**, *13* (24), 7271−7279.
(54) Kessel, D. Death Pathways Associated with Photodynamic Therapy. *Photochem. Photobiol.* **2006**, *21* (4), 219−224.
(55) Notte, A.; Leclere, L.; Michiels, C. Autophagy as a Mediator of Chemotherapy-Induced Cell Death in Cancer. *Biochem. Pharmacol.* **2011**, *82* (5), 427−434.
(56) Kondo, Y.; Kanzawa, T.; Sawaya, R.; Kondo, S. The Role of Autophagy in Cancer Development and Response to Therapy. *Nat. Rev. Cancer* **2005**, *5* (9), 726−734.
(57) Cuervo, A. M. Autophagy: In Sickness and in Health. *Trends Cell Biol.* **2004**, *14* (2), 70−77.
(58) Chen, Y.; McMillan-Ward, E.; Kong, J.; Israels, S. J.; Gibson, S. B. Oxidative Stress Induces Autophagic Cell Death Independent of Apoptosis in Transformed and Cancer Cells. *Cell Death Differ.* **2008**, *15* (1), 171−182.
(59) Xu, Y.; Kim, S. O.; Li, Y.; Han, J. Autophagy Contributes to Caspase-Independent Macrophage Cell Death. *J. Biol. Chem.* **2006**, *281* (28), 19179−19187.
(60) Nikoletopoulou, V.; Markaki, M.; Palikaras, K.; Tavernarakis, N. Crosstalk between Apoptosis, Necrosis and Autophagy. *Biochim. Biophys. Acta, Mol. Cell Res.* **2013**, *1833* (12), 3448−3459.
(61) Massagué, J.; Obenauf, A. C. Metastatic Colonization by Circulating Tumour Cells. *Nature* **2016**, *529* (7586), 298−306.
(62) Welch, D. R.; Hurst, D. R. Defining the Hallmarks of Metastasis. *Cancer Res.* **2019**, *79* (12), 3011−3027.
(63) Weng, X.; Wei, D.; Yang, Z.; Pang, W.; Pang, K.; Gu, B.; Wei, X. Photodynamic Therapy Reduces Metastasis of Breast Cancer by Minimizing Circulating Tumor Cells. *Biomed. Opt. Express* **2021**, *12* (7), 3878−3886.
(64) Wang, W.; Moriyama, L. T.; Bagnato, V. S. Photodynamic Therapy Induced Vascular Damage: An Overview of Experimental PDT. *Laser Phys. Lett.* **2013**, *10* (2), No. 023001.
(65) Khurana, M.; Moriyama, E. H.; Mariampillai, A.; Samkoe, K.; Cramb, D.; Wilson, B. C. Drug and light dose responses to focal photodynamic therapy of single blood vessels in vivo. *J. Biomed. Opt.* **2009**, *14* (6), No. 064006.
(66) Towers, C. G.; Wodetzki, D.; Thorburn, A. Autophagy and Cancer: Modulation of Cell Death Pathways and Cancer Cell Adaptations. *J. Cell Biol.* **2020**, *219* (1), No. e201909033.

https://doi.org/10.1021/acsomega.1c07046
ACS Omega 2022, 7, 17563−17574

(67) Sharifi, M. N.; Mowers, E. E.; Drake, L. E.; Collier, C.; Chen, H.; Zamora, M.; Mui, S.; Macleod, K. F. Autophagy Promotes Focal Adhesion Disassembly and Cell Motility of Metastatic Tumor Cells through the Direct Interaction of Paxillin with LC3. *Cell Rep.* **2016**, *15* (8), 1660−1672.
(68) Kenific, C. M.; Stehbens, S. J.; Goldsmith, J.; Leidal, A. M.; Faure, N.; Ye, J.; Wittmann, T.; Debnath, J. NBR1 Enables Autophagy-Dependent Focal Adhesion Turnover. *J. Cell Biol.* **2016**, *212* (5), 577−590.
(69) Fong, M. H. Y.; Feng, M.; McConkey, D. J.; Choi, W. Update on Bladder Cancer Molecular Subtypes. *Transl. Androl. Urol.* **2020**, *9* (6), 2881−2889.
(70) Wang, S.; Jin, S.; Shu, Q.; Wu, S. Strategies to Get Drugs across Bladder Penetrating Barriers for Improving Bladder Cancer Therapy. *Pharmaceutics* **2021**, *13* (2), 166.
(71) Imani, R.; Veranič, P.; Iglič, A.; Kreft, M. E.; Pazoki, M.; Hudoklin, S. Combined Cytotoxic Effect of UV-Irradiation and TiO2Microbeads in Normal Urothelial Cells, Low-Grade and High-Grade Urothelial Cancer Cells. *Photochem. Photobiol. Sci.* **2015**, *14* (3), 583−590.
(72) Foggi, C. C.; Fabbro, M. T.; Santos, L. P. S.; de Santana, Y. V. B.; Vergani, C. E.; Machado, A. L.; Cordoncillo, E.; Andrés, J.; Longo, E. Synthesis and Evaluation of α-Ag2WO4 as Novel Antifungal Agent. *Chem. Phys. Lett.* **2017**, *674*, 125−129.
(73) Borra, R. C.; Lotufo, M. A.; Gagioti, S. M.; Barros, F. de M.; Andrade, P. M. A Simple Method to Measure Cell Viability in Proliferation and Cytotoxicity Assays. *Braz. Oral Res.* **2009**, *23* (3), 255−262.
(74) Parra-Robert, M.; Casals, E.; Massana, N.; Zeng, M.; Perramón, M.; Fernández-Varo, G.; Morales-Ruiz, M.; Puntes, V.; Jiménez, W.; Casals, G. Beyond the Scavenging of Reactive Oxygen Species (ROS): Direct Effect of Cerium Oxide Nanoparticles in Reducing Fatty Acids Content in an In Vitro Model of Hepatocellular Steatosis. *Biomolecules* **2019**, *9* (9), 425.
(75) Rafehi, H.; Orlowski, C.; Georgiadis, G. T.; Ververis, K.; El-Osta, A.; Karagiannis, T. C. Clonogenic Assay: Adherent Cells. *J. Vis. Exp.* **2011**, *49*, 2573.
(76) Yue, P. Y. K.; Leung, E. P. Y.; Mak, N. K.; Wong, R. N. S. A Simplified Method for Quantifying Cell Migration/Wound Healing in 96-Well Plates. *J. Biomol. Screen.* **2010**, *15* (4), 427−433.
(77) Yarrow, J. C.; Perlman, Z. E.; Westwood, N. J.; Mitchison, T. J. A High-Throughput Cell Migration Assay Using Scratch Wound Healing, a Comparison of Image-Based Readout Methods. *BMC Biotechnol.* **2004**, *4*, 21.
(78) Cossarizza, A.; Chang, H.-D.; Radbruch, A.; Akdis, M.; Andrä, I.; Annunziato, F.; Bacher, P.; Barnaba, V.; Battistini, L.; Bauer, W. M.; Baumgart, S.; Becher, B.; Beisker, W.; Berek, C.; Blanco, A.; Borsellino, G.; Boulais, P. E.; Brinkman, R. R.; Büscher, M.; Busch, D. H.; Bushnell, T. P.; Cao, X.; Cavani, A.; Chattopadhyay, P. K.; Cheng, Q.; Chow, S.; Clerici, M.; Cooke, A.; Cosma, A.; Cosmi, L.; Cumano, A.; Dang, V. D.; Davies, D.; De Biasi, S.; Del Zotto, G.; Della Bella, S.; Dellabona, P.; Deniz, G.; Dessing, M.; Diefenbach, A.; Di Santo, J.; Dieli, F.; Dolf, A.; Donnenberg, V. S.; Dörner, T.; Ehrhardt, G. R. A.; Endl, E.; Engel, P.; Engelhardt, B.; Esser, C.; Everts, B.; Dreher, A.; Falk, C. S.; Fehniger, T. A.; Filby, A.; Fillatreau, S.; Follo, M.; Förster, I.; Foster, J.; Foulds, G. A.; Frenette, P. S.; Galbraith, D.; Garbi, N.; García-Godoy, M. D.; Geginat, J.; Ghoreschi, K.; Gibellini, L.; Goettlinger, C.; Goodyear, C. S.; Gori, A.; Grogan, J.; Gross, M.; Grützkau, A.; Grummitt, D.; Hahn, J.; Hammer, Q.; Hauser, A. E.; Haviland, D. L.; Hedley, D.; Herrera, G.; Herrmann, M.; Hiepe, F.; Holland, T.; Hombrink, P.; Houston, J. P.; Hoyer, B. F.; Huang, B.; Hunter, C. A.; Iannone, A.; Jäck, H.-M.; Jávega, B.; Jonjic, S.; Juelke, K.; Jung, S.; Kaiser, T.; Kalina, T.; Keller, B.; Khan, S.; Kienhöfer, D.; Kroneis, T.; Kunkel, D.; Kurts, C.; Kvistborg, P.; Lannigan, J.; Lantz, O.; Larbi, A.; LeibundGut-Landmann, S.; Leipold, M. D.; Levings, M. K.; Litwin, V.; Liu, Y.; Lohoff, M.; Lombardi, G.; Lopez, L.; Lovett-Racke, A.; Lubberts, E.; Ludewig, B.; Lugli, E.; Maecker, H. T.; Martrus, G.; Matarese, G.; Maueröder, C.; McGrath, M.; McInnes, I.; Mei, H. E.; Melchers, F.; Melzer, S.; Mielenz, D.; Mills, K.; Mirrer, D.; Mjösberg, J.; Moore, J.; Moran, B.; Moretta, A.; Moretta, L.; Mosmann, T. R.; Müller, S.; Müller, W.; Münz, C.; Multhoff, G.; Munoz, L. E.; Murphy, K. M.; Nakayama, T.; Nasi, M.; Neudörfl, C.; Nolan, J.; Nourshargh, S.; O'Connor, J.-E.; Ouyang, W.; Oxenius, A.; Palankar, R.; Panse, I.; Peterson, P.; Peth, C.; Petriz, J.; Philips, D.; Pickl, W.; Piconese, S.; Pinti, M.; Pockley, A. G.; Podolska, M. J.; Pucillo, C.; Quataert, S. A.; Radstake, T. R. D. J.; Rajwa, B.; Rebhahn, J. A.; Recktenwald, D.; Remmerswaal, E. B. M.; Rezvani, K.; Rico, L. G.; Robinson, J. P.; Romagnani, C.; Rubartelli, A.; Ruckert, B.; Ruland, J.; Sakaguchi, S.; Sala-de-Oyanguren, F.; Samstag, Y.; Sanderson, S.; Sawitzki, B.; Scheffold, A.; Schiemann, M.; Schildberg, F.; Schimisky, E.; Schmid, S. A.; Schmitt, S.; Schober, K.; Schüler, T.; Schulz, A. R.; Schumacher, T.; Scotta, C.; Shankey, T. V.; Shemer, A.; Simon, A.-K.; Spidlen, J.; Stall, A. M.; Stark, R.; Stehle, C.; Stein, M.; Steinmetz, T.; Stockinger, H.; Takahama, Y.; Tarnok, A.; Tian, Z.; Toldi, G.; Tornack, J.; Traggiai, E.; Trotter, J.; Ulrich, H.; van der Braber, M.; van Lier, R. A. W.; Veldhoen, M.; Vento-Asturias, S.; Vieira, P.; Voehringer, D.; Volk, H.-D.; von Volkmann, K.; Waisman, A.; Walker, R.; Ward, M. D.; Warnatz, K.; Warth, S.; Watson, J. V.; Watzl, C.; Wegener, L.; Wiedemann, A.; Wienands, J.; Willimsky, G.; Wing, J.; Wurst, P.; Yu, L.; Yue, A.; Zhang, Q.; Zhao, Y.; Ziegler, S.; Zimmermann, J. Guidelines for the Use of Flow Cytometry and Cell Sorting in Immunological Studies. *Eur. J. Immunol.* **2017**, *47* (10), 1584−1797.
(79) Martins, W. K.; Severino, D.; Souza, C.; Stolf, B. S.; Baptista, M. S. Rapid Screening of Potential Autophagic Inductor Agents Using Mammalian Cell Lines. *Biotechnol. J.* **2013**, *8* (6), 730−737.
(80) Thomé, M. P.; Filippi-Chiela, E. C.; Villodre, E. S.; Migliavaca, C. B.; Onzi, G. R.; Felipe, K. B.; Lenz, G. Ratiometric Analysis of Acridine Orange Staining in the Study of Acidic Organelles and Autophagy. *J. Cell Sci.* **2016**, *129* (24), 4622−4632.
(81) Scaduto, R. C.; Grotyohann, L. W. Measurement of Mitochondrial Membrane Potential Using Fluorescent Rhodamine Derivatives. *Biophys. J.* **1999**, *76* (1), 469−477.
(82) Fujita, N.; Nagahashi, A.; Nagashima, K.; Rokudai, S.; Tsuruo, T. Acceleration of Apoptotic Cell Death after the Cleavage of Bcl-XL Protein by Caspase-3-like Proteases. *Oncogene* **1998**, *17* (10), 1295−1304.

https://doi.org/10.1021/acsomega.1c07046
ACS Omega 2022, 7, 17563−17574